Video Article

Formation of Thick Dense Yttrium Iron Garnet Films Using Aerosol Deposition

Scooter D. Johnson[1], Evan R. Glaser[2], Fritz J. Kub[1], Charles R. Eddy, Jr.[1]

[1]Power Electronics Branch, Naval Research Laboratory

[2]Physics of Electronic Materials Branch, Naval Research Laboratory

Correspondence to: Scooter D. Johnson at scooter.johnson.ctr@nrl.navy.mil

URL: https://www.jove.com/video/52843
DOI: doi:10.3791/52843

Keywords: Engineering, Issue 99, aerosol deposition, yttrium iron garnet, microwave materials, radio frequency materials, thick film, ferromagnetic resonance, cold spray coating, room temperature, ceramics, multifunctional materials, ferrites, oxides

Date Published: 5/15/2015

Citation: Johnson, S.D., Glaser, E.R., Kub, F.J., Eddy, Jr., C.R. Formation of Thick Dense Yttrium Iron Garnet Films Using Aerosol Deposition. *J. Vis. Exp.* (99), e52843, doi:10.3791/52843 (2015).

Abstract

Aerosol deposition (AD) is a thick-film deposition process that can produce layers up to several hundred micrometers thick with densities greater than 95% of the bulk. The primary advantage of AD is that the deposition takes place entirely at ambient temperature; thereby enabling film growth in material systems with disparate melting temperatures. This report describes in detail the processing steps for preparing the powder and for performing AD using the custom-built system. Representative characterization results are presented from scanning electron microscopy, profilometry, and ferromagnetic resonance for films grown in this system. As a representative overview of the capabilities of the system, focus is given to a sample produced following the described protocol and system setup. Results indicate that this system can successfully deposit 11 μm thick yttrium iron garnet films that are > 90% of the bulk density during a single 5 min deposition run. A discussion of methods to afford better control of the aerosol and particle selection for improved thickness and roughness variations in the film is provided.

Video Link

The video component of this article can be found at https://www.jove.com/video/52843/

Introduction

Aerosol deposition (AD) is a thick-film deposition process that can produce layers up to several hundred micrometers thick with densities greater than 95% of the bulk[1]. The deposition process is believed to occur through a continual process of impact, fracture or deformation, adhesion, and densification of particles. **Figure 1** depicts this process as a series of steps showing particle impact and densification over several steps. As shown, the particles move toward the substrate with a typical velocity of 100–500 m/sec. As the initial particles impact with the substrate they fracture and adhere to the substrate. This anchoring layer provides the mechanical adhesion between the substrate and the bulk film. As subsequent impacts occur the underlying particles are increasingly fractured, adhered, and further densified. This process of continual impact, fracture, and densification works to compact the underlying film and bond the crystallites and produce a film with a density reaching greater than 95% of the bulk material.

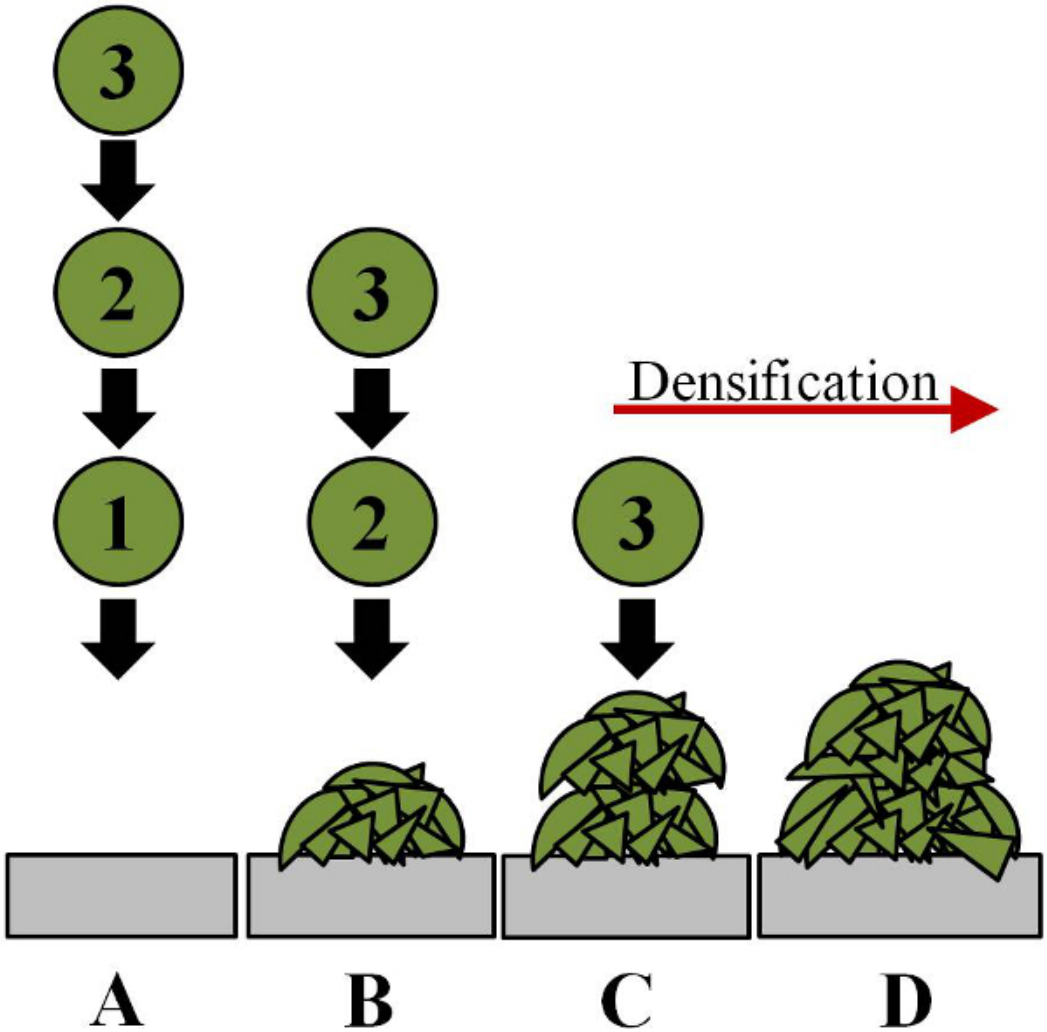

Figure 1. Illustration of the deposition process. Panel A shows three particles moving toward the substrate with a typical velocity of 100–500 m/sec. Panel B shows the result of impact, fracture, and adhesion of the first particle. Panels C and D show the subsequent impact of the second and third particles, which further compact the underlying film and bond the crystallites. The result is a film with density greater than 95% of the bulk material (reproduced with permission from Reference 19). Please click here to view a larger version of this figure.

The primary advantage of AD is that the deposition takes place entirely at ambient RT; thereby enabling film growth, for instance, of a high-melting-temperature material (starting powder) onto a low-melting-temperature substrate. The deposition rate can be up to several micrometers per minute and is performed at moderate vacuum conditions of 1–20 Torr in the deposition chamber. The process shows the ability to scale up to very large deposition areas and finally, it can deposit conformally.[2]

There are many material systems studied by AD for a wide variety of uses, such as inductors[3], abrasion-resistant coatings[4], piezoelectrics[5], multiferroics[6], magnetoelectrics[7] thermistors[8], thermoelectric films[9], flexible dielectrics[10], hard tissue implants and bioceramics[11], solid electrolytes[12], and photocatalysts[13]. For applications to microwave devices, magnetic films of several hundreds of micrometers in thickness are required that would ideally be integrated directly into the circuit board elements. One challenge to realizing this integration is the high-temperature regime needed for fabricating ferrite films (see review by Harris *et al.*[14]), such as yttrium iron garnet (YIG). For this reason AD appears to be a natural choice for realizing potential new advancements in magnetic integrated circuit technology. The low-cost operation, high deposition rate, and simplicity of AD has spurred interest by researchers in Germany, France, Japan, Korea, and now in the United States.

Figure 2 is a drawing outlining the basic setup to perform aerosol deposition. Pressure is monitored at the locations marked P_{AC}, P_{DC}, and P_H for the aerosol chamber, deposition chamber, and pump head, respectively. The gas flow, controlled by the mass flow controller (MFC), enters the aerosol chamber and aerosolizes the powder. The deposition chamber is pumped to create the pressure difference between the two chambers, causing the flow of particles through the rectangular (0.4 mm x 4.8 mm) nozzle opening.

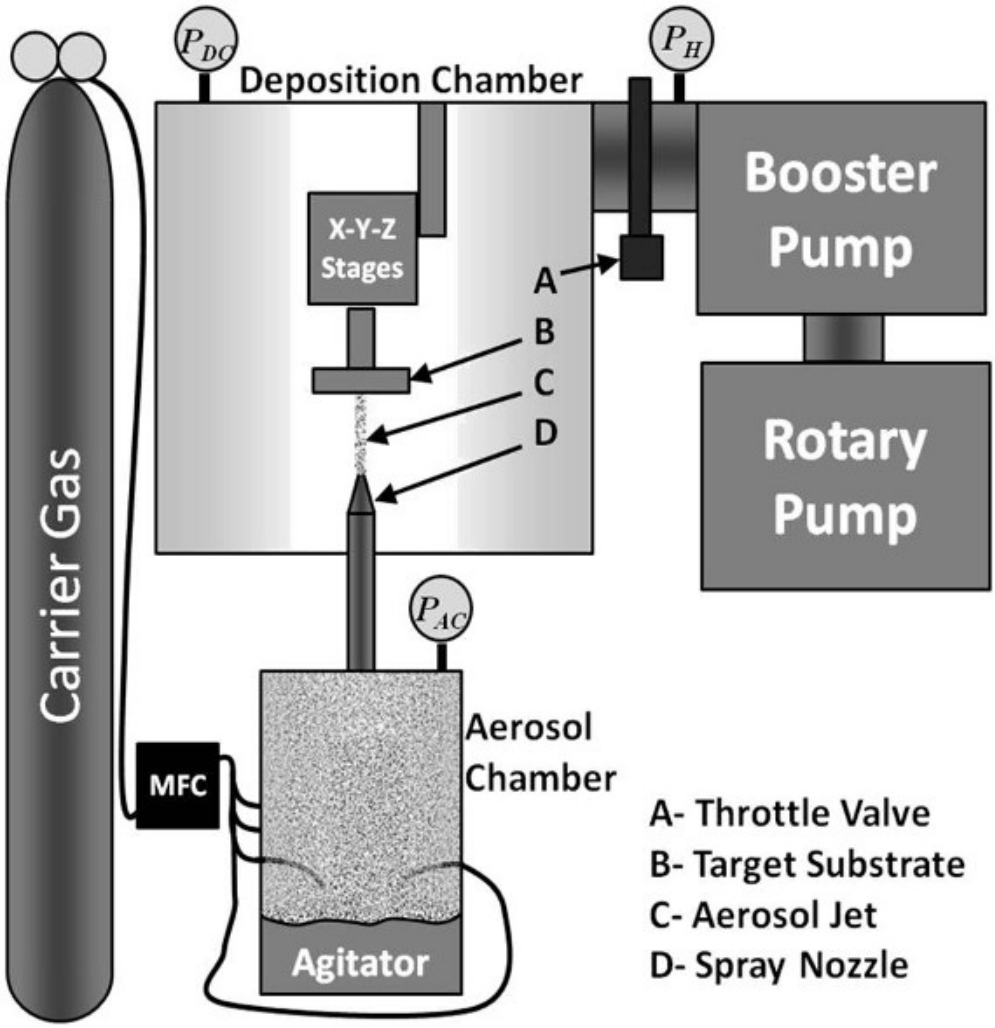

Figure 2. Main components in the NRL ADM system. Pressure is monitored at the locations marked P_{AC}, P_{DC}, and P_H for the aerosol chamber, deposition chamber, and pump head, respectively. See text for details. (copyright (2014) The Japan Society of Applied Physics, reproduced from Reference 20). Please click here to view a larger version of this figure.

The average size of an individual YIG particle in this work is 0.5 µm. The effect of agglomeration causes these small particles to form much larger agglomerates that range in size from about 10 µm to about 400 µm. Control of the agglomerate size and delivery rate is essential to achieving a dense well-formed film. This necessitates configuration of an aerosol chamber that allows size selection and uniform particle flux into the deposition chamber. The powder is pre-sieved to remove any agglomerates larger than 53 µm prior to being loaded into the aerosol chamber. The aerosol chamber configuration used in this work is illustrated in **Figure 3**. Nitrogen gas enters through four inlet nozzles (two are shown in **Figure 3**) located at the bottom sides of the chamber. The gas interacts with the YIG powder (shown in green) to produce an aerosol comprised of a distribution of agglomerated particle sizes less than 53 µm. An agitator at the base of the aerosol chamber made of a stainless steel plate is vibrated continuously to keep the powder moving into the gas flow. The agglomerates impact a 45 µm filter, allowing only agglomerates sized less than 45 µm to enter the nozzle inlet. Upon entering the nozzle inlet the agglomerates are accelerated to a large velocity and ejected into the deposition chamber (not shown) to perform the deposition. A stainless steel rod connects the bottom of the filter to the base of the agitator (not shown) to aid in de-clogging the filter.

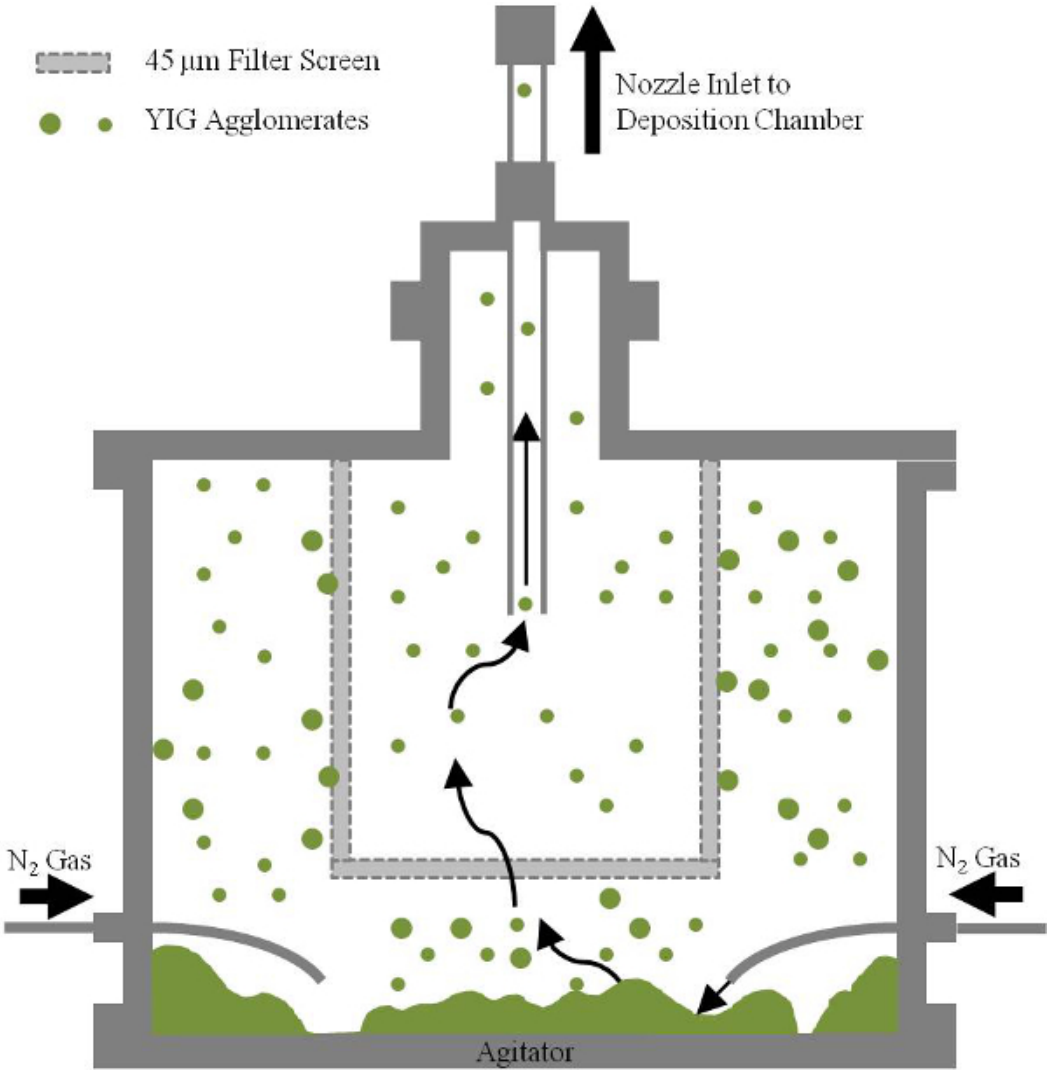

Figure 3. Illustration of the internal aerosol chamber configuration, with filter, inlet nozzles, and YIG powder shown. See text for details.

This report details the experimental procedure to perform AD using the custom-built system described above to produce dense films of YIG. Representative results for an 11 µm thick film produced in this system are presented using scanning electron microscopy (SEM), thickness profiles, and ferromagnetic resonance (FMR). The results presented are not intended to be an in-depth study of the magnetic properties or material structure of the film, but as a demonstration of the films produced by this technique. Please click here to view a larger version of this figure.

Protocol

1. Powder Preparation

1. Sieve as-received yttrium iron garnet (YIG) powder to obtain 100–150 g of agglomerates sized less than 53 µm.
2. Place the sieved powder into a furnace to dry for at least 24 hr at a temperature greater than 300 °C.

2. Substrate Preparation

1. Clean a substrate of desired size, *e.g.*, 3 mm x 3 mm using acetone then isopropanol. Dry using nitrogen gas.

3. Performing Aerosol Deposition

1. Mount the sample to the translation mounting stage.
    1. Place double-sided copper tape to the mounting stage. Place the cleaned substrate onto the copper tape.
    2. Measure the distance from the edge of the mounting stage to each edge of the sample. Record the dimensions and sample position on the sample history sheet.

3. Check that the mounting stage is aligned parallel with the body of the translation motor by measuring the distance from the edge of the mounting stage to the edge of the motor body with calipers. Load the sample into the deposition chamber.
4. Clamp the flange to seal the deposition chamber. Attach the 3 15-pin D-sub controller cables for the translation motors.

2. Load the powder and close up the aerosol chamber.
   1. Remove the dried powder from the furnace and place it in the aerosol chamber bottom section. Slide the filter de-clogging rod attachment onto the filter de-clogging rod.
   2. Place the main body of the aerosol chamber onto the aerosol chamber bottom section. Allow the filter de-clogging rod attachment to rest on the agitation plate as the main body is being attached to the bottom section.
   3. Clamp the main body to the bottom section. Attach the aerosol chamber pressure gauge to the side port on the main body of the aerosol chamber.
   4. Clamp the nozzle inlet section to the top port on the main body of the aerosol chamber using a QF clamp. Raise the nozzle inlet tube to the inlet port on the deposition chamber and secure the top and bottom fitting.
   5. Record the powder and aerosol chamber identification numbers on the sample history sheet.
3. Turn on the roughing pump with it isolated from the rest of the system. Turn on the deposition chamber illumination lamp. Open the constriction valve on the bypass line to begin the pump-down of the entire system.
4. Setup the pressure monitoring software with the deposition run identification.
5. Run the stage controller macro creator by typing ‘pitrans’ in the command line terminal window and enter the requested information. Create a new sheet in the run log spreadsheet and record the deposition parameters and setup notes.
6. After the system pressure has reached about 150–200 Torr, slightly open the unconstricted valve. Maintain a pump-down rate of about 1 Torr/sec. Once the pressure has dropped below 100 Torr start the pressure monitoring software and the translation stage motor controller software.
7. Once the system pressure has reached about 1 Torr close all three valves to the bypass line and open the main pumping valve. Tighten the clamp to the top cap on the deposition chamber.
8. Turn on the blower pump. Open the ultra-high purity (UHP) nitrogen gas cylinder. Monitor the pressure and record the base pressure of the system (it typically reaches 15–25 mTorr).
9. Set the distance between the nozzle and the substrate. Use the stage controller software graphical user interface window to move the mounted substrate over the nozzle. Lower the substrate until it contacts the nozzle. Move the substrate 7.5 mm in the vertical direction from this position.
10. Close the main pumping line and monitor the leak rate of the system on the pressure monitoring software. Note the initial leak rate upon shutting the valve. If this leak rate is less than 3.33 mTorr/sec continue, otherwise begin checking for leaks. A typical leak rate is less than 1.2 mTorr/sec.
11. Set the deposition chamber butterfly valve to the 500 Torr preset value. Set the mass flow controller value to 13.63 L/min (do not turn it on).
12. Move the mounting stage to the starting position for the deposition. Load the macro created in step 3.7 into the controller software.
13. Program the function generator to sweep linearly between 135 and 145 Hz every 10 sec. Turn the function generator on. Turn the nitrogen gas flow on. After a 3 sec countdown start the stage controller macro.
14. Monitor the deposition and adjust gas flow rate as necessary to keep the pressure difference at 500 ± 0.5 Torr (or as desired for the run) for the duration of the deposition.
    Note: The pressure in the deposition chamber is typically 0.65 Torr and the pressure in the deposition chamber is typically 501 Torr. Uncontrollable variations in pressure usually indicate that the UHP nitrogen is running out. A slight drop in pressure (1–2 Torr) over the duration of the run is typical. This can be remedied by increasing the gas flow rate. During the initial passes a visible film should form on the substrate, lack of film formation suggests insufficient aerosolization of the powder and/or significant filter clogging.
15. At the end of the deposition note the exact deposition run time. Shut off the nitrogen gas, the function generator, and the pumps. Open the deposition chamber butterfly valve completely.
16. Open the bypass valve located at the side of the deposition chamber. Turn the house nitrogen gas regulator to zero and redirect it into the deposition chamber. Close the main pumping valve while slowly increasing the house gas regulator pressure.
17. Home the nozzle to X = 25 mm, Y = 25 mm, and Z = 25 mm, then close the stage controller software.
18. Once the pressure in the system has risen above 100 Torr stop the pressure monitoring software. Record the total nitrogen gas used and time to complete the deposition. Adjust the house gas pressure as necessary until the system reaches atmosphere.
19. Unplug the 3 15-pin D-sub stage controller cables and unclamp the top cap. Remove the top cap from the deposition chamber and unmount the sample.

4. Post-deposition Inspection

1. Remove the sample from the mounting stage and inspect it under a microscope. If necessary, wash the sample in isopropanol to remove loose powder. Perform the planned characterizations of the film.

Representative Results

After the deposition is complete, the coated substrates are removed from the deposition chamber and inspected using an optical stereo microscope. Samples are typically brushed and washed with isopropanol to remove excess powder that remained during re-pressurization to atmosphere. Film characterization was performed on the representative results presented here using scanning electron microscopy to assess the morphology of the film, profilometry to assess the film thickness, uniformity, and roughness, and ferromagnetic resonance to assess the magnetic properties of the film (see Reference 20 for additional details on the characterization methods). In this study, a 3 mm x 3 mm sapphire substrate was coated using the above protocol and system setup. The deposition sweep was set to raster across the film at 0.65 mm/sec and to cover a total area of 75 mm^2.

Figure 4 is an SEM image of the top surface of the film showing many small grains that are much smaller than the starting size of the individual particles (0.5 µm). It is evident from the image that the film has formed a somewhat rough, well-compacted surface with very few voids. For films of similar results presented here we have measured the density to between 90%–96% of the theoretical density for YIG (5.17 g/cm^3). The cross-sectional view of the film shown in **Figure 5** also supports the dense nature of the film. The main image in **Figure 5** shows the edge of the as-deposited sample as formed during deposition, *i.e.*, it is not a cleaved section of the film. The inset shows a magnified view of the cross-section of the film indicating the dense nature of the film. We have also performed X-ray diffraction on the as-deposited films and starting powder and found that the crystal structure does not change upon deposition (data not shown; see also References 3 and 20).

Figure 6 is a plot of the step height of the film. The total area of the sample is 3 mm x 3 mm (the total deposition area was 75 mm^2). The step was created by removing a portion of the film along one edge of the substrate. The red line overlaying the data indicates the average film thickness of 10.93 µm by averaging three profile scans across the film. The rms roughness R_q = 1.37 µm. The deposition time to form this film was 337 sec, resulting in a deposition rate of 1.95 µm/min.

Figure 7 is a plot of the FMR absorption derivative taken at RT: data shown in black. A Lorentzian derivative lineshape fit to the data is shown in red. The linewidth of the data is 330 Oe and the resonance field is 2,810 Oe. The signal location and shape is comparable to a typical spectrum for polycrystalline YIG grown by other methods, *e.g.*, pulsed laser deposition or rf magnetron sputtering[15,16]. The Lorentzian lineshape gives a good fit to the data suggesting a uniform film[17,18].

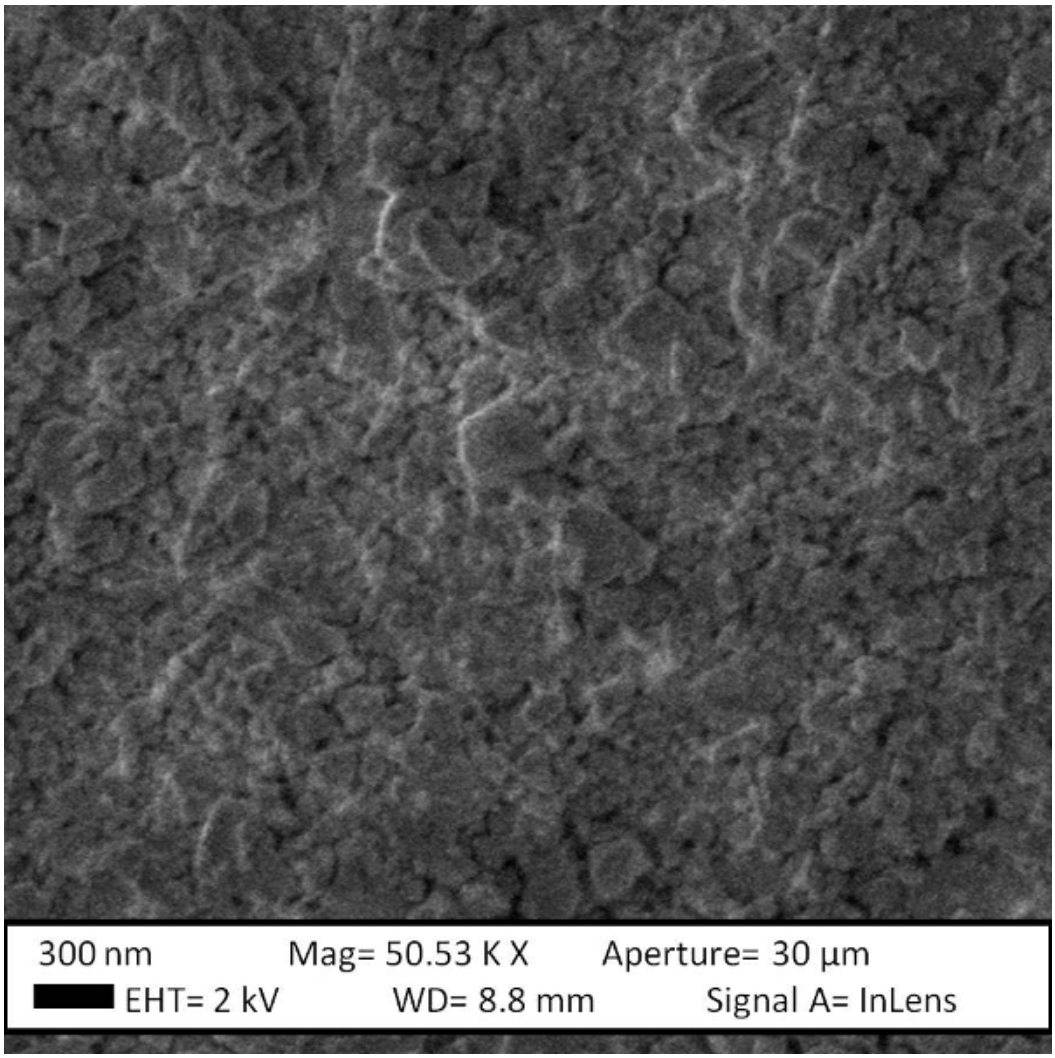

Figure 4. SEM image of the top surface of the film post-deposition. The image shows a film with many grains that are densely compacted and much smaller than the 0.5 µm individual starting particle size. Please click here to view a larger version of this figure.

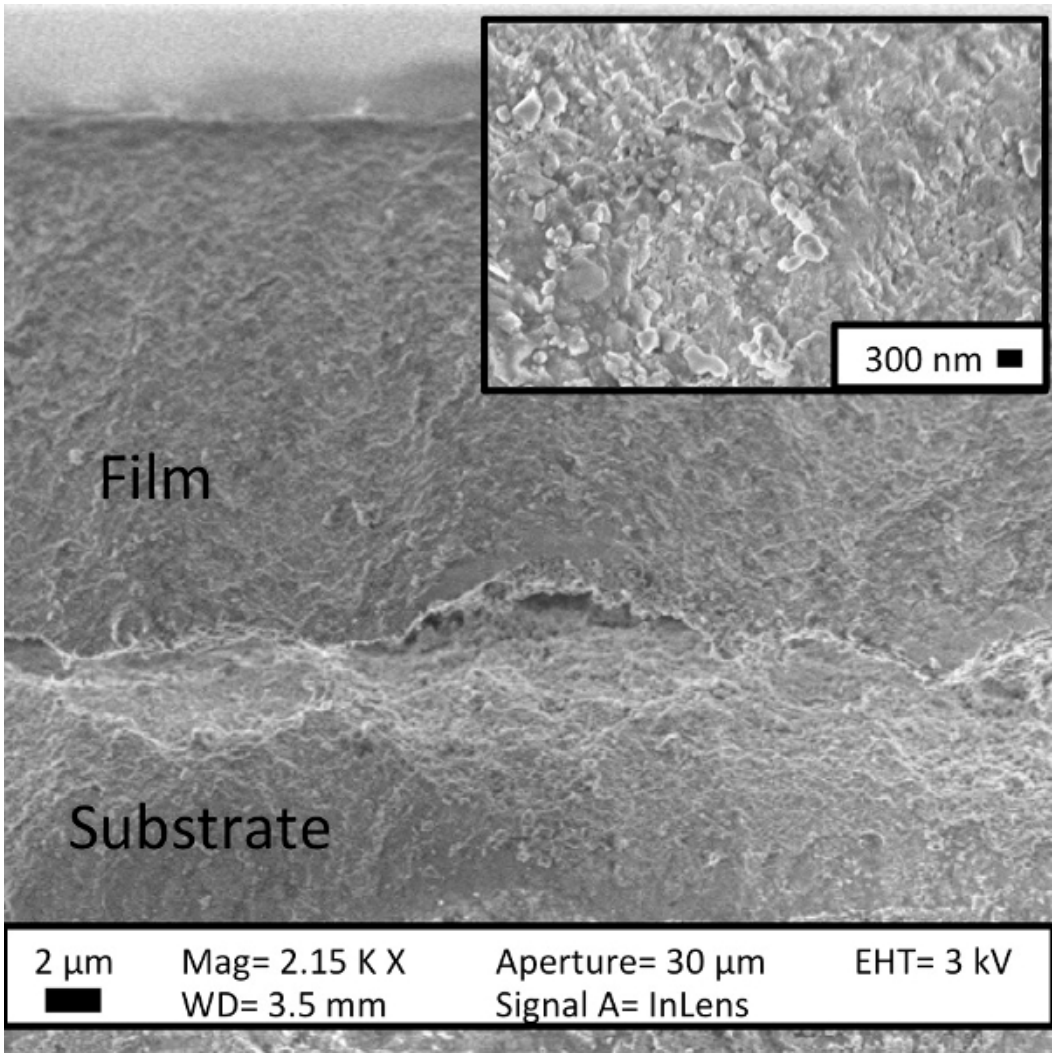

Figure 5. SEM image of the cross-section of the film on the sapphire substrate. The inset is a magnified view of the cross-section of the film. Please click here to view a larger version of this figure.

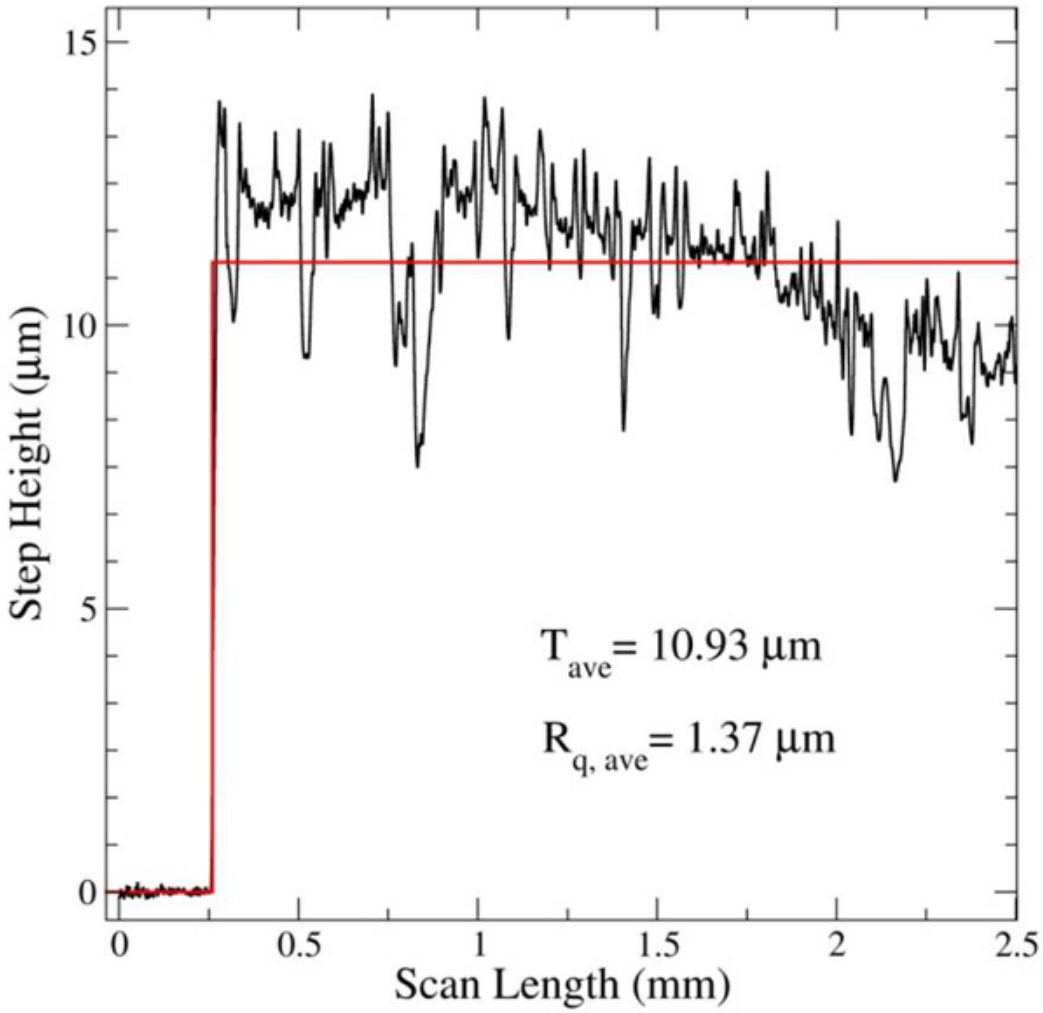

Figure 6. A representative step profile of the film in Figure 4 and Figure 6 showing the variation in thickness across 2.25 mm of the 3 mm total length of the sample. The average thickness of 10.93 µm is shown as the red line overlaying the data. Please click here to view a larger version of this figure.

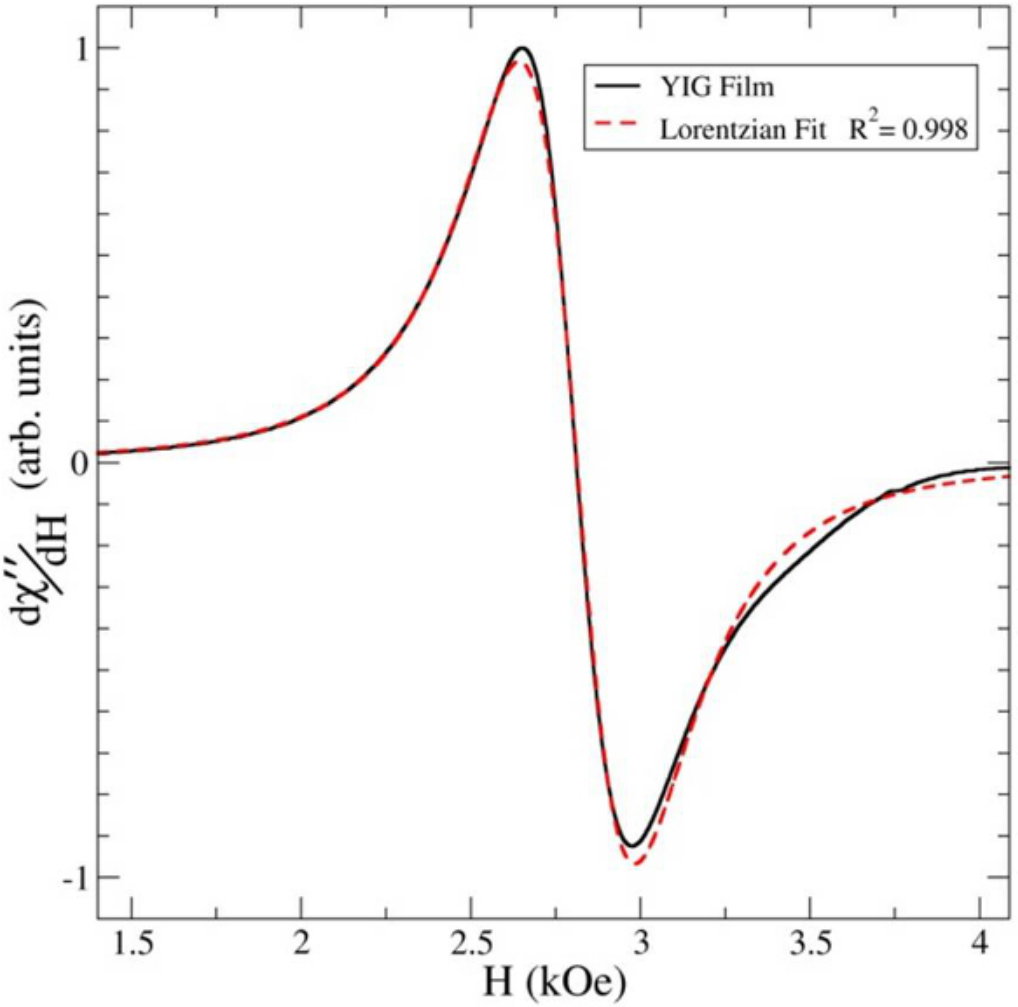

Figure 7. Ferromagnetic resonance derivative curve of the film taken at RT. The spectrum is well fit by a Lorentzian function indicating a uniform homogenous film. The linewidth is 330 Oe. Please click here to view a larger version of this figure.

Discussion

The SEM image in **Figure 4** indicates that significant fracture and densification is occurring during the deposition process. The image is taken of the top surface of the film, which shows a small number of voids and grains. The observable region is the last of the material to be deposited and therefore does not benefit from the further impact and densification process of subsequent particles as illustrated by impact from particle 2 and 3 in **Figure 1**. The film density within the volume of the sample can be seen by the cross-sectional image in **Figure 5**. This image, along with the higher magnification inset of the cross-section, provides further evidence for a dense film.

The roughness seen in the SEM image is also confirmed quantitatively in the profile scans. The roughness of these films may be due to the high rate of deposition (1.95 µm/min). It is possible that films formed more slowly will enable particles to fully fracture and adhere before additional particles arrive, but the increase in film roughness may also be fundamentally related to the increase in film thickness[21]. The drop in the thickness across the film suggests that the particle flow into the deposition chamber is not constant during the entire deposition. Possible reasons could stem from loss of powder in the aerosol, clumping of the powder at the base of the aerosol chamber, and/or filter clogging. Fully drying and sieving the powders and modifying the aerosol chamber to that shown in **Figure 3** are strategies undertaken to improve and control the deposition rate and film uniformity.

The FMR spectrum for this sample indicates that the YIG film has a resonance field and lineshape that is typical of polycrystalline YIG films grown by other techniques. The linewidth of the AD deposited film is somewhat wider than other reported polycrystalline films by about 100–200 Oe[16]. This is likely due to the nano-crystalline make-up of the film. Note that single-crystal YIG films have a typical FMR linewidth of less than 1 Oe even for comparable thicknesses [22]. Since this film is well-modeled by a Lorentzian lineshape one might conclude that the film is uniform and free from inhomogeneities. In this case, the broadening of the linewidth could be attributed to intrinsic relaxation processes such as Gilbert dampening and/or 2-magnon scattering[18]. The sloping thickness profile in **Figure 6** is evidence that the deposition rate is not constant throughout the process, and therefore, the film is not likely to be completely free from inhomogeneities. A more in-depth study needs to be undertaken to fully implicate these mechanisms (see also discussion in Ref. 3), as well as, better refinement of the current AD system. The most likely cause of the non-uniform coverage is that the aerosol generated in the aerosol chamber may become depleted and/or the filter becomes

clogged. Both of these effects would cause the amount of powder entering the deposition chamber to diminish and thereby result in a lower deposition rate.

The results presented above indicate successful deposition of a nearly 11 µm thick film at a deposition rate of nearly 2 µm/min (for a 75 mm^2 area) using the AD system and protocol presented here. The film is comprised of densely compacted and randomly oriented grains that are much smaller than the starting particles due to the impact, fracture and densification mechanisms involved in this process. The film shows comparable FMR linewidth shape and resonance field to reported YIG films [15-17]. Additional work to better control the flow of agglomerates into the deposition chamber is needed to ensure more uniform film growth.

Current work is underway to further improve the consistency of the deposition process. Additional drying and sieving protocols are being developed to ensure that the powder has the same consistency during each run. Designs are also underway to create an improved filtration system with less clogging. A redesign of the nozzle inlet will also aid in preventing clumped powder from collecting within the nozzle neck. More in-depth studies of the magnetic and structural properties are also underway. Some current studies include, building up films layer-by-layer to better understand variations in the magnetic properties of these films created by aerosol deposition.

Disclosures

The authors have nothing to disclose.

Acknowledgements

SDJ gratefully acknowledges the support of the American Association for Engineering Education/NRL Postdoctoral Fellowship Program, discussions with Konrad Bussmann (NRL) and Mingzhong Wu (Colorado State University) on the magnetic properties of materials, and Ron Holm (NRL) for his part in the design and implementation of the NRL AD system.

References

1. Akedo, J. Room Temperature Impact Consolidation (RTIC) of Fine Ceramic Powder by Aerosol Deposition Method and Applications to Microdevices. *J. of Therm. Spray tech.* **17**, 181 (2008).
2. Hahn, B. D., Park, D. -S., Choi, J. -J., Ryu, J. Osteoconductive hydroxyapatite coated PEEK for spinal fusion surgery. *Appl. Surf. Sci.* **283**, 6-11 (2013).
3. Johnson, S. D., *et al.* Aerosol Deposition of Yttrium Iron Garnet for Fabrication of Ferrite-Integrated On-Chip Inductors. *IEEE Trans. on Magnetics.* **51**, (05), (2015).
4. Johnson, S. D., Kub, F. J., Eddy, C. R. ZnS/Diamond Composite Coatings for Infrared Transmission Applications Formed by the Aerosol Deposition Method. *Proceedings of SPIE.* **8708**, 87080T-87081T (2013).
5. Han, G., Ryu, J., Yoon, W. -H., Choi, J. -J. Effect of electrode and substrate on the fatigue behavior of PZT thick. *Ceram. Int.* **38**, (1), S241-S244 (2012).
6. Ryu, J., Baek, C. -W., Lee, Y. -S., Oh, N. -K. Enhancement of Multiferroic Properties in BiFeO3-Ba(Cu1/3Nb2/3)O-3. *Film. J. Am. Ceram. Soc.* **94**, (2), 355-358 (2011).
7. Park, C. -S., Ryu, J., Choi, J. -J., Park, D. -S. Giant Magnetoelectric Coefficient in 3-2 Nanocomposite Thick Films. *Jpn. J. Appl. Phys.* **48**, (8), 1 (2009).
8. Ryu, J., Park, D. -S., Schmidt, R. In-plane impedance spectroscopy in aerosol deposited NiMn2O4 negative. *J. Appl. Phys.* **109**, (11), 112722 (2011).
9. Yoon, W. -H., Ryu, J., Choi, J. -J., Hahn, B. -D. Enhanced Thermoelectric Properties of Textured Ca3Co4O9 Thick Film by Aerosol Deposition. *J. Am. Ceram. Soc.* **93**, (8), 2125-2127 (2010).
10. Ryu, J., Kim, K. -Y., Choi, J. -J., Hahn, B. -D. Flexible Dielectric Bi1.5Zn1.0Nb1.5O7 Thin Films on a Cu-Polyimide Foil. *J. Am. Ceram. Soc.* **92**, (2), 524-527 (2009).
11. Hahn, B. -D., Lee, J. -M., Park, D. -S., Choi, J. -J. Mechanical and in vitro biological performances of hydroxyapatite-carbon. *Acta Biomater.* **8**, (8), 3205-3214 (2009).
12. Choi, J. -J., Cho, K. -S., Choi, J. -H., Ryu, J. Effects of annealing temperature on solid oxide fuel cells containing (La,Sr) (Ga,Mg,Co)O3-δ electrolyte prepared by aerosol deposition. *Mater. Lett.* **70**, 44-47 (2012).
13. Ryu, J., Hahn, B. -D. Porous Photocatalytic TiO2 Thin Films by Aerosol Deposition. *J. Am. Ceram. Soc.* **93**, (1), 55-58 (2010).
14. Harris, V. G., *et al.* Recent advances in processing and applications of microwave ferrites. *J. of Magn. and Magn. Mat.* **321**, 2035 (2009).
15. Kang, Y. -M., Ulyanov, A. N., Yoo, S. -I. FMR linewidths of YIG films fabricated by ex situ post-annealing of amorphous films deposited by rf magnetron sputtering. *Phys. Stat. Sol. (a).* **204**, (3), 763-767 (2007).
16. Popova, E., *et al.* Perpendicular magnetic anisotropy in ultrathin yttrium iron garnet films prepared by pulsed laser deposition technique). *J. of Vac. Sci. Techn. A.* **19**, (5), 2567-2570 (2001).
17. Sun, Y., *et al.* Growth and ferromagnetic resonance properties of nanometer-thick yttrium. *Appl. Phys. Lett.* **101**, (15), 082405 (2012).
18. Kalarickal, S. S., Krivosik, P., Das, J., Kim, K. S., Patton, C. E. Microwave damping in polycrystalline Fe-Ti-N films: Physical mechanisms and correlations with composition and structure. *Phys. Rev. B.* **77**, 054427 (2008).
19. Johnson, S. D. Advances in Ferrite-Integrated On-Chip Inductors Using Aerosol Deposition. *Magnetics Business & Technology Magazine.* **10**, (2014).
20. Johnson, S. D., Glaser, E. R., Cheng, S. -F., Kub, F., Eddy Jr,, R, C. Characterization of As-Deposited and Sintered Yttrium Iron Garnet Thick Films Formed by Aerosol. *Appl. Phys. Express.* **7**, 035501 (2014).
21. Lee, D. -W., Nam, S. -M. Factors Affecting Surface Roughness of Al2O3 Films Deposited on Cu Substrates by an Aerosol Deposition Method. *J. of Ceramic Proc. Research.* **11**, 100 (2010).

22. Glass, H. L., Elliott, M. T. Attainment of the Intrinsic FMR Linewidth in Yttrium Iron Garnet Films Grown by Liquid Phase Epitaxy.J. *Cryst. Growth.* **34**, 285 (1976).

